Research Paper

GEOSPHERE

GEOSPHERE

https://doi.org/10.1130/GES02549.1

5 figures; 1 table

CORRESPONDENCE:
glevresse@geociencias.unam.mx

CITATION: Billarent-Cedillo, A., Hernandez-Pérez, E., Levresse, G., Inguaggiato, C., Ferrari, L., Inguaggiato, S., Lopez-Alvis, J., and Silva-Fragoso, A., 2022, Mantellic degassing of helium in an extensional active tectonic setting at the front of a magmatic arc (central Mexico): Geosphere, https://doi.org/10.1130/GES02549.1.

Science Editor: Christopher J. Spencer
Associate Editor: Julie Roberge

Received 10 May 2022
Revision received 5 August 2022
Accepted 6 October 2022

Published online 12 December 2022

Mantellic degassing of helium in an extensional active tectonic setting at the front of a magmatic arc (central Mexico)

Andrea Billarent-Cedillo[1,*], Eliseo Hernandez-Pérez[1], Gilles Levresse[2], Claudio Inguaggiato[3], Luca Ferrari[2], Salvatore Inguaggiato[4], Jorge López-Alvis[2], and Argelia Silva-Fragoso[2]

[1]Posgrado en Ciencias de la Tierra, UNAM Campus Juriquilla, Boulevard Juriquilla 3001, Querétaro 76230, México
[2]Centro de Geociencias, UNAM Campus Juriquilla, Boulevard Juriquilla 3001, Querétaro 76230, México
[3]Departamento de Geología, Centro de Investigación Científica y de Educación Superior de Ensenada (CICESE), Carretera Ensenada-Tijuana 3918, Ensenada, Baja California, México
[4]Istituto Nazionale di Geofisica e Vulcanologia, Sezione di Palermo, via Ugo La Malfa, 143, 90145 Palermo, Italy

ABSTRACT

The physicochemical and isotopic characteristics of groundwater and dissolved gas of central Mexico provide valuable information about the geologic and tectonic context of the area. Low–high-enthalpy manifestations (up to 98 °C in springs and more than 100 °C in geothermal wells) are distributed within the San Juan del Río, Querétaro, and Celaya hydrologic basins, located at the boundary between the current Mexican magmatic arc and an extensional continental area with intraplate volcanism called Mesa Central Province. Groundwaters in the study area represent a mixture between the cold water end-member with a Ca^{2+}-Mg^{2+}-HCO_3- composition and a hydrothermal end-member enriched in Na^+, K^+, SO_4^{2-}, and Cl-. Cold and hot groundwaters δ^2H and $\delta^{18}O$ plot along the same evaporation lines and do not exhibit a magmatic input. Dissolved and free gas do not show a typical volcanic composition signature. He and Ne isotope composition provide evidence of an important contribution of non-atmospheric noble gases. Although helium composition mainly has a crustal origin (21–83%), the mantellic contribution (1–39%) is higher than expected for an area lacking recent volcanism. A volatile-rich magma aging at depth was discarded as the source of this mantellic helium signature but points out a recent mantellic contribution. Thus, we propose that mantellic helium comes from the sublithospheric mantle into the shallow crust through the highly permeable tectonic boundaries between the geologic provinces, namely the N–S Taxco–San Miguel de Allende and Chapala-Tula fault systems. Mantellic helium flow rates through these fault systems were estimated to have values ranging from 0.1 m/yr to 2.9 m/yr. This He flux range implies that aside from subduction, mantle volatile degassing enhanced by crustal fault systems is the main degassing process in the region studied.

INTRODUCTION

The origin of volatiles emitted from convergent and passive margins provides fundamental constraints on how plate tectonics redistributes fluids between terrestrial reservoirs (Hilton et al., 2002; Plank et al., 2013; Bekaert et al., 2021). In continental regions, helium isotopic composition is mainly dominated by its heavy isotope, ^4He, as a consequence of the radioactive decay of the U-Th–enriched continental crust (O'Nions and Oxburgh, 1988; Tolstikhin and Marty, 1998; Ballentine and Burnard, 2002; Ray et al., 2009). Although this is not quite true in active tectonic regions, an important ^3He input from the mantle melts to the crust can be recognized (Ballentine and Burnard, 2002). These regions are basically active continental arcs that function as conduits of mantle or magmatic material to the surface (Hilton et al., 2002), or major tectonic boundaries, such as the San Andreas fault (Kennedy et al., 1997; Kulongoski et al., 2013) and the New Zealand Alpine fault (Giggenbach et al., 1993; Menzies et al., 2016).

Fluid flow is the dominant process associated with the transport of mass and energy in the crust. Mantle volatiles play an important role in lithospheric rheology. Heat and mass are injected into the shallow crust when buoyant mantle fluids are able to flow through the ductile lower crust (Kennedy and van Soest, 2007). Even though the lower crust is considered an impermeable boundary due to the inability to maintain open fractures over long time scales (Byerlee, 1993), fluid transit may occur through punctual magma intrusion and degassing or by diffusion (Torgersen, 1993). Both of these methods are not very effective, and volatile fluxes are generally quite limited. However, along crustal boundaries, fault-controlled advective flow of mantle fluids through the ductile crust has been reported (Ballentine et al., 2005; Kulongoski et al., 2005). In such a case, extensive circulation of fluids is generally possible in the upper crust under hydrostatic pressure, driven by thermal or compositional gradients (Yardley and Bodnar, 2014). In magmatic arcs, fluids are intrinsically linked to tectonic processes, which favor the connection between deep and shallow fluid reservoirs and provide key structural pathways for fluids. In these complex environments, shallow waters buffer the deep fluid flow. However, in highly fractured areas with deep structures, the intensity of deep fluid flow increases, which provides a less diluted signature and the opportunity to estimate its inflow (Tardani et al., 2016; Buttitta et al., 2020).

In central Mexico, the active magmatic arc has a geographically well-defined extension called the Trans-Mexican Volcanic Belt. To the north, the Trans-Mexican Volcanic Belt faces the Mesa Central Province that is

gilles levresse https://orcid.org/0000-0001-9290-9825
*Current affiliation: Department of Earth Sciences, Utrecht University, Utrecht 3584,The Netherlands

characterized, among other things, by current intraplate volcanism. The contact zone between subduction-related magmatism and intraplate magmatism is fuzzy and marked by numerous unconventional low–medium enthalpy geothermal anomalies. On the surface, both subduction and intraplate volcanism are active but structurally controlled by crustal structures of incompatible directions (Hernández-Pérez et al., 2022). At depth, the extension to the north of the metasomatism of the mantle wedge of subduction is difficult to estimate, as is the participation of the two types of magmatism in the generation of thermal anomalies.

In this study, we analyze the possible sources and pathways for crustal and mantle fluids in a range of high–low enthalpy hydrothermal springs from the San Juan del Río–Querétaro–Celaya Valley region, which lies at the northern border of the active magmatic arc (the Trans-Mexican Volcanic Belt) and its intersection with the major crustal boundary of the San Miguel Allende–Taxco fault system (Figs. 1A and 1B).

REGIONAL GEOLOGICAL SETTING

The study area is located at the intersection of three geologic provinces: the Trans-Mexican Volcanic Belt, the Mesa Central, and the Sierra Madre Oriental (Fig. 1A). The Trans-Mexican Volcanic Belt is a large Neogene continental arc that grows over the central Mexican margin of the North American Plate as a result of the subduction of the Rivera and Cocos plates along the Middle America Trench (Ferrari et al., 2012). The Trans-Mexican Volcanic Belt is composed of nearly 8000 igneous structures that extend from the coast of Jalisco to the Gulf of Mexico in Veracruz. The Trans-Mexican Volcanic Belt is divided into three sectors (Gómez-Tuena et al., 2005). The western sector contains the Chapala, Tepic-Zaocoalco, and Colima rifts, which bound the Jalisco block. The central sector includes the San Miguel de Allende–Taxco fault system and the Michoacan-Guanajuato monogenetic Pleistocene volcanic fields and is bounded to the north by the Mesa Central Province. The eastern sector extends from the San Miguel Allende–Taxco fault system to the Gulf of Mexico. The seismic contours of the slab show that the Cocos Plate is sub-horizontal at the south of the Trans-Mexican Volcanic Belt. Below the Trans-Mexican Volcanic Belt the slab shows a different dip between the central and eastern sectors; it is steeper eastward (up to ~75°) (Fig. 1A). The slab is also affected by trench orthogonal tears and is truncated at ~500 km (Fig. 1A; Pérez-Campos et al., 2008; Husker and Davis, 2009; Kim et al., 2010). The truncation of the slab seen in the seismic tomography in the central Trans-Mexican Volcanic Belt occurs just below the northern boundary of the Trans-Mexican Volcanic Belt and coincides with the Bajío fault and the Chapala-Tula fault system (Fig. 1A; Botero-Santa et al., 2015). The Mesa Central Province is an elevated plateau located 2000 m above sea level in central Mexico, which has undergone several episodes of magmatism and extension from the Paleocene to the Pleistocene (Nieto-Samaniego et al., 1999; Del Pilar-Martínez et al., 2020). The Sierra Madre Oriental, the highest mountain chain in northeastern Mexico (Fig. 1A), is composed of marine sedimentary rocks of Middle Jurassic to Paleogene age. It is part of the Mexican fold-and-thrust belt that developed between the Late Cretaceous and early Eocene (Fitz-Díaz et al., 2018). Its western part is covered by volcanic and pyroclastic rocks of the Cenozoic Sierra Madre Occidental silicic large igneous province, whereas to the south it is covered by the Trans-Mexican Volcanic Belt.

The San Miguel Allende–Taxco fault system and the Chapala-Tula fault system are major crustal structural boundaries between the Mesa Central and Sierra Madre Oriental provinces and the Trans-Mexican Volcanic Belt (Fig. 1C; Alaniz-Álvarez and Nieto-Samaniego, 2005). The southern extension of the San Miguel Allende–Taxco fault system is the limit between the central and western sectors of the Trans-Mexican Volcanic Belt. The intersection between the Mesa Central, Sierra Madre Oriental, and Trans-Mexican Volcanic Belt geologic provinces is characterized by important variations in crustal thickness. In fact, the crustal thickness decreases from ~40 km to 50 km in the Trans-Mexican Volcanic Belt to ~37 km in the Sierra Madre Oriental Province and ~32 km in the Mesa Central Province (Fig. 1A). A low degree of partial melting has been interpreted from seismic studies just below the Moho in the southern Mesa Central Province and the northern part of the Trans-Mexican Volcanic Belt, which suggests that the addition of molten materials at the base of the crust produced an uplift and heating of the lower and middle part of the crust (Nieto-Samaniego et al., 1999; Ferrari et al., 2012, and references therein).

The San Miguel Allende–Taxco fault system (Alaniz-Álvarez et al., 2002) and the Chapala-Tula fault system (Aguirre-Díaz et al., 2005) intersect orthogonally in the San Juan del Río–Querétaro–Celaya region (Figs. 1B and 1C). The study area lies on the northern part of the Trans-Mexican Volcanic Belt and displays some recent volcanism (>40,000 years) in the Michoacán-Guanajuato volcanic field (Luhr et al., 2006; Gómez-Vasconcelos et al., 2020) and upper crustal historical seismicity at the Sanfandila fault (Aguirre-Díaz and McDowell, 2000; Zúñiga et al., 2003). This region is also geothermally active, with two high-enthalpy fields at Los Azufres and at Celaya, as well as several low–medium enthalpy anomalies distributed within the central Trans-Mexican Volcanic Belt (Fig. 1; González-Guzmán et al., 2019; Jácome-Paz, 2019; Pérez-Martínez et al., 2020, and references therein).

The stratigraphic column comprises rocks from the Jurassic to Quaternary. The oldest rock units are a middle Jurassic volcano-sedimentary succession (ca. 100 Ma; Ochoa-González et al., 2015) and Late Cretaceous limestone (Palacios-García and Martini, 2014) exposed in the northeastern part of the area (Fig. 1B). This Mesozoic basement succession is sheared and folded and unconformably overlain by Oligocene to Quaternary volcanic rocks (Alaniz-Álvarez et al., 2001; Verma and Carrasco-Núñez, 2003; Arango-Guevara et al., 2007). The transition between the deformed basement and the Cenozoic volcanics is highlighted by a continental conglomerate of Eocene age (Aguirre-Díaz and McDowell, 2000; Aranda-Gómez and McDowell, 1998). The oldest volcanic pulse is Rupelian in age and is part of the major pulse of ignimbrite flare-up of the Sierra Madre Occidental large igneous province (Aguirre-Díaz and López-Martínez, 2001; Ferrari et al., 2018). It includes pyroclastic flow

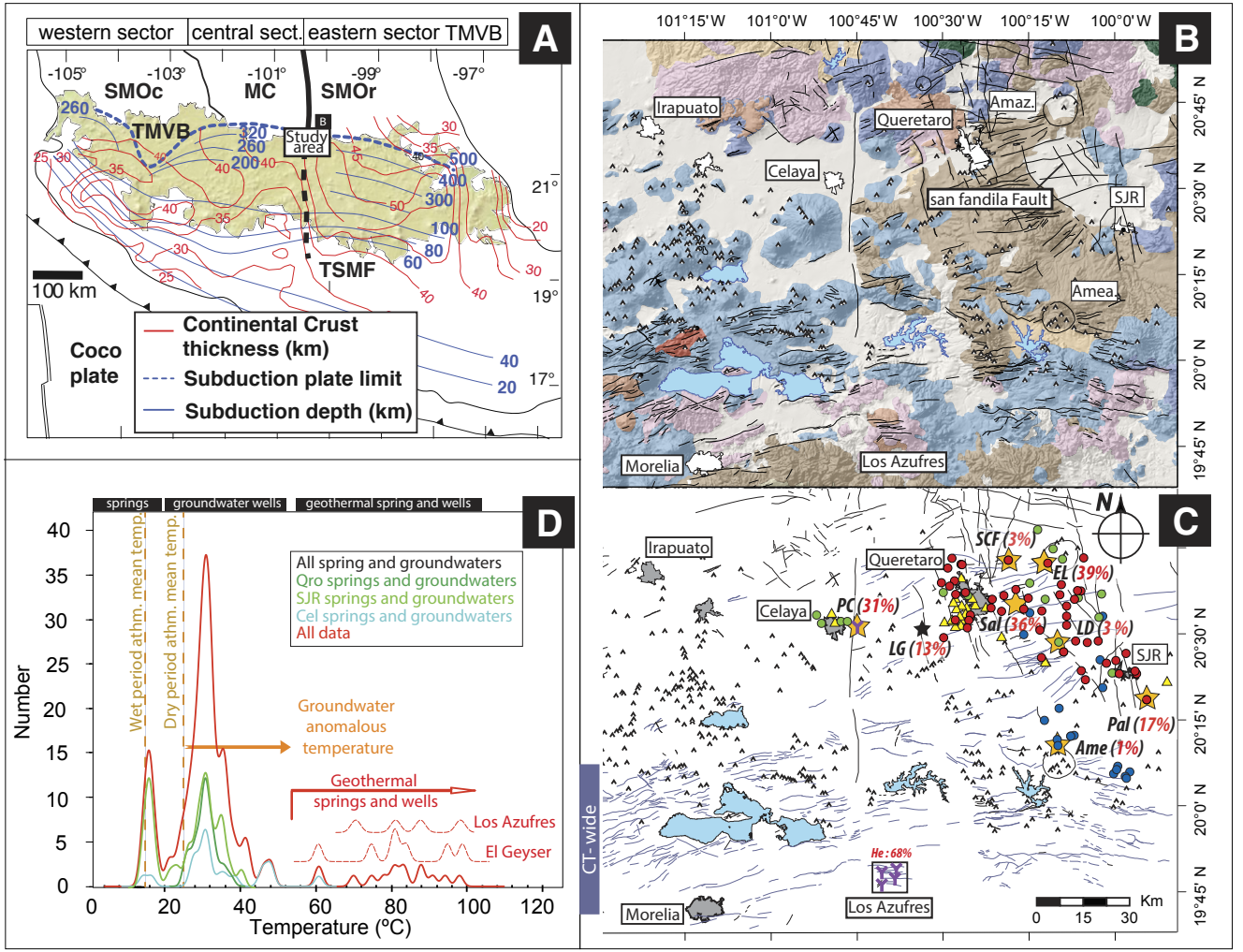

Figure 1. (A) Tectonic setting of central and southern Mexico is shown. The white box indicates the main focus area of this study. The black contour lines depict the depth of the subducted slab compiled using the results of receiver functions, tomography studies, and hypocentral relocalization (from Ferrari et al., 2012). The dashed blue line represents the limit of the subduction plate. The red line illustrates the thickness of the crust beneath and south of the Trans-Mexican Volcanic Belt (in kilometers) (Ferrari et al., 2012, and references therein). The Trans-Mexican Volcanic Belt (TMVB) is delimited by the green area (from Ferrari et al., 2012). SMOc—Sierra Madre Occidental Province; MC—Mesa Central Province; SMOr—Sierra Madre Oriental Province; TSMF—Taxco San Miguel fault. (B) Simplified geological map of the study area. (C) Simplified structural map with sampling sites marked. SCF, PC, LG, Sal, EL, LD, Pal, and Ame are sample names. CT—Chapala-Tula. (D) Temperature distribution of water sampled from rain, springs, and groundwaters (low-temperature groundwater and high-temperature groundwater) of the San Juan del Río (SJR) Basin. The vertical orange dashed lines correspond to the average atmospheric temperature of the dry (21 °C) and wet (17 °C) period. In panel B: SJR—San Juan del Río city; Amea.—Amealco caldera; Amaz.—Amazcala caldera. Percentage in red indicates the mantellic helium contribution of each sample. SMAT—San Miguel Allende–Taxco.

deposits, rhyolite domes, and lava flows, which are commonly observed discordantly overlying the deformed Mesozoic rocks. The Rupelian volcanic event is followed by a Miocene volcanic succession concurrent with the development of extensional fault systems, which is locally faulted and affected by hydrothermal alteration. The Miocene volcanism began with the emplacement of andesitic to dacitic polygenetic volcanoes dated at ca. 13–10 Ma (Pérez-Venzor et al., 1996; Valdez-Moreno et al., 1998; Verma and Carrasco-Núñez, 2003) and was followed by mafic lava flows forming an extensive plateau, a few shield volcanoes, and monogenetic cinder cones with ages ranging from 8.8 Ma to 7.5 ± 0.5 Ma (Aguirre-Díaz and López-Martínez, 2001; Dávalos-Álvarez et al., 2005), which are mostly exposed in the Querétaro and San Juan del Río areas. Shortly after, at ca. 7.3 Ma, the volcanic activity become bimodal with the formation of the Amazcala rhyolitic caldera (Aguirre-Díaz and López-Martínez, 2001) and less voluminous fissural mafic lavas east of Querétaro. During the Pliocene (5–4.2 Ma), volcanism moves toward the southeast, with the development of the Amealco dacitic caldera and a massive rhyolitic dome complex southwest of the San Juan del Río basin (Aguirre-Díaz, 1996; Aguirre-Díaz and López-Martínez, 2009). Additional silicic volcanism occurred at the Los Azufres caldera, in the southern part of the study area, with rhyolitic ignimbrites, domes, and pyroclastic flows from the Pliocene to Holocene (Ferrari et al., 1991; Arce et al., 2021). To the west, basaltic and basaltic andesite monogenetic cones, shield volcanoes, and a few domes were emplaced in the Michoácan-Guanajuato volcanic field (Hasenaka and Carmichael, 1985; Hasenaka, 1994). Fluvial, lacustrine, alluvial deposits, and unconsolidated volcano-sedimentary and pyroclastic rocks fill the Miocene–present tectonic basins (Alaniz-Álvarez et al., 2001).

METHODS

Samples for dissolved and noble gas analysis were selected from the extensively evaluated published and personal database of physicochemical parameters of the groundwaters and spring waters from the Celaya, Querétaro, and San Juan del Río basins (see Results section) to obtain a representative panorama of the varied occurrence of groundwater types and the impact/recording of deep-flow fluids within them.

Six water samples (SCF, Sal, EL, LD, Ame, and PAL) were collected from urban wells in the Querétaro and San Juan del Río basins (25–300 m), and one gas sample (PC) was collected from a geothermal well in Celaya. The waters have an abnormally high temperature except for the Ame sample, which has a much lower temperature (20.7 °C), which is close to the average atmospheric temperature. Physicochemical parameters (temperature, pH, electrical conductivity, and oxidation-reduction potential) were measured in situ using a Thermo Scientific® Orion 5-Star Plus multiparameter analyzer that was calibrated before sampling. Water $^{18}O/^{16}O$ and $^{2}H/H$ isotope ratios (expressed in δ-notation normalized relative to the Vienna Standard Mean Ocean Water) were analyzed at the Laboratorio de Isotopía Estable of the Instituto de Geología, UNAM, using the Los Gatos Research DLT-100 V3® isotope ratio laser spectrometer (IRLS). The standard deviation for the $\delta^{18}O$ was less than ± 0.2‰ and less than ± 2‰ for the $\delta^{2}H$‰. All of the hydrochemical data, including the $\delta^{18}O$ and $\delta^{2}H$‰, are reported in Supplemental Material Table S1[1].

Water samples were collected in 121 ml glass bottles to analyze the chemical composition of gases and helium isotopes dissolved in water (Capasso and Inguaggiato, 1998; Inguaggiato and Rizzo, 2004). The glass samplers were completely filled with water and sealed underwater with rubber septa to prevent air contamination during the sampling procedure. The method used to analyze dissolved gases is based on the equilibrium partition of gases between the water phase collected and the gas phase (Capasso and Inguaggiato, 1998; Inguaggiato and Rizzo, 2004). The sample bottles were immersed in water to prevent air contamination during storage. A free gas sample was collected at the geothermal well in Celaya city.

Analysis of the chemical composition of gases and the noble gas isotopic composition was conducted at the geochemical laboratory of the Istituto Nazionale di Geofisica e Vulcanologia–Palermo (INGV-Pa) in Italy. The chemical composition of dissolved gases was analyzed by an Agilent 7890 gas chromatograph using Ar as the carrier gas. The gas chromatograph is equipped with two detectors: a thermal conductivity detector (TCD) for the analysis of He, H_2, O_2, and N_2, and a flame ionization detector (FID) for the analysis of CO, CO_2, and CH_4. A detailed description of the methods used for gas extraction and dissolved gas analysis can be found in Capasso and Inguaggiato (1998). The analytical error was less than 5%.

The ^{3}He, ^{4}He, and ^{20}Ne isotopic concentrations were measured to calculate the $^{3}He/^{4}He$ and $^{4}He/^{20}Ne$ ratios. Noble gases were purified from the gas mixture in a stainless steel ultra-high vacuum line and then cryogenically separated and admitted into a split-flight tube noble-gas mass spectrometer (GVI™ Helix SFT) for He isotopes and into a noble gas multicollector mass spectrometer (Helix MC Plus™ Multicollector) for Ne isotopes. A multicollector mass spectrometer (GVI™ Helix MC) was used to analyze Ar (Rizzo et al., 2015). The method for gas extraction and isotopic analyses is described in detail in Inguaggiato and Rizzo (2004). The analytical error was less than 3% on a single mass. The concentration of dissolved gases is expressed as cm^3/g at 0 °C and 1 atm (STP). The helium isotope ratios are reported as R/Ra, where R is the $^{3}He/^{4}He$ ratio determined in the sample and Ra is the atmospheric one (1.39×10^{-6}). The R/Ra values were corrected for atmospheric contamination (Rc/Ra) using the air normalized $^{4}He/^{20}Ne$ ratio equation of Hilton (1996).

$$\frac{R_C}{R_a} = \frac{\left(\frac{R}{R_a} * X\right) - 1}{X - 1} \quad (1)$$

[1]Supplemental Material. Table S1: Physicochemical parameters and composition of rain, spring and groundwater in the Celaya, Querétaro and San Juan del Río aquifers. Please visit https://doi.org/10.1130/GEOS.S.21513981 to access the supplemental material, and contact editing@geosociety.org with any questions.

$$\text{where } X = \frac{\left(\frac{He}{Ne}\right)_{sample}}{\left(\frac{He}{Ne}\right)_{air}} \frac{\beta_{Ne}}{\beta_{He}} \quad (2)$$

and β_{Ne} and β_{He} are the Bunsen solubility coefficients for Ne and He, respectively, at the temperature and salinity of the water when the atmospheric helium was dissolved. Only in the case of the gas sample PC, which was not dissolved in water, the ratio of β_{Ne} and β_{He} was not used to calculate (Rc/Ra), and X is $(He/Ne)_{sample}/(He/Ne)_{air}$. R/Ra values of the LD and Amealco 1 samples were not corrected for air contamination as their $^4He/^{20}Ne$ value is <25% higher than the $^4He/^{20}Ne$ value of air, which implies a significant error for the correction.

RESULTS

Regional Hydrological System Re-Evaluation

The study area comprises three connected hydrologic basins: the San Juan del Río, Querétaro, and Celaya basins (Figs. 1B and 1C). The hydraulic basins of San Juan del Río and Querétaro comprise the hydraulic head of the Lerma and Panuco regional basins. The piezometric gradient continually decreases from the San Juan del Río to the Celaya aquifer. However, the average temperature of the aquifers continually increases from San Juan del Río to Celaya. These aquifers can be defined as compartmentalized and multi-layer, in which granular and fractured layers with contrasting hydraulic properties, as well as several structural discontinuities, influence the groundwater flow dynamics (Carrera-Hernández et al., 2016; López-Alvis et al., 2019; Hernández-Pérez et al., 2020). Groundwater is thermally anomalous (with respect to mean air temperature of 18 °C; Fig. 1D) with localized geothermal spring occurrences along N–S structures (i.e., El Geyser and Celaya geothermal well; González-Guzmán et al., 2019) and hydro-chemically heterogeneous with F^-, As, and Li^+ punctual anomalies (González-Guzmán et al., 2019; Amézaga-Campos et al., 2022). For comparison, we include physicochemical data from the Los Azufres geothermal field (Fig. 2). All of the physicochemical data, from the study area plus the regional geothermal field (Los Azufres; González-Partida et al., 2005; Pinti et al., 2013), were used to perform a hierarchical cluster and principal component analysis (PCA) to discriminate the different types of the sampling waters. The results derived from the PCA are presented in Figure 2. Seven main clusters were identified using a dissimilarity index of 7, selected based

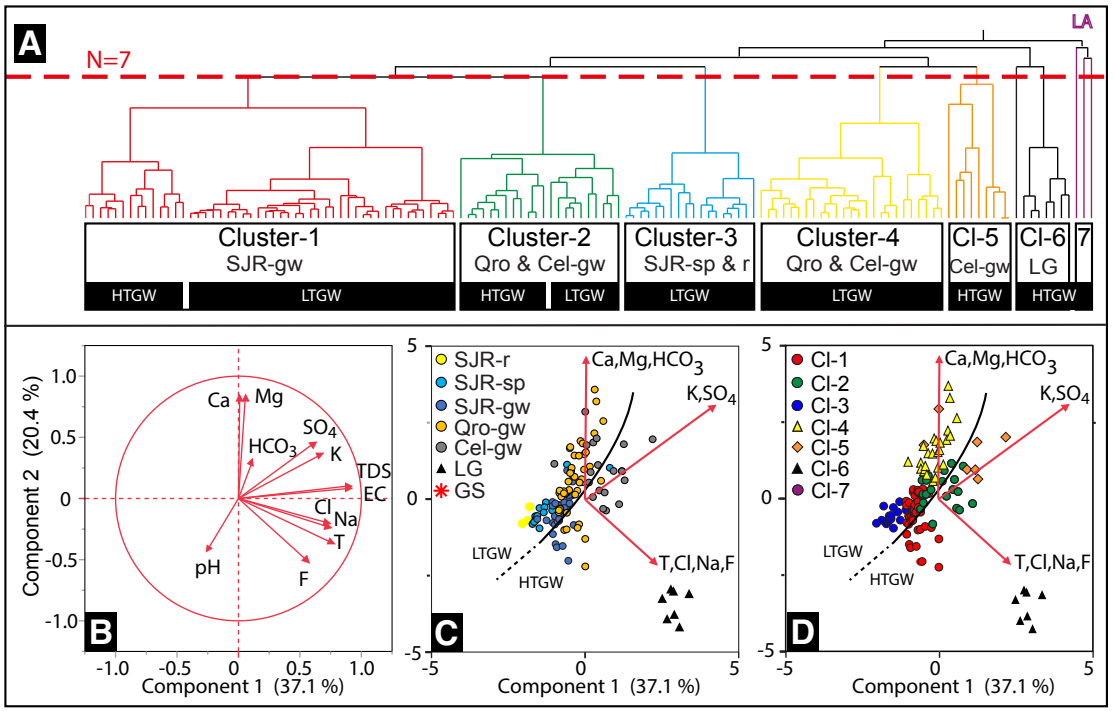

Figure 2. (A) Dendrogram shows Hierarchical Clustering Analysis classification with groups and subgroups of samples of the San Juan del Río, Querétaro, and Celaya aquifers (Hernández-Pérez et al., 2022; González-Guzmán et al., 2019; Amézaga-Campos et al., 2022). For comparison, temperature and chemical data from the Los Azufres geothermal field are presented (LA; González-Partida et al., 2005). (B) Load distribution for Component 1 and Component 2 of the analysis variables in the San Juan del Río Basin. (C) Principal component analysis (PCA) diagram differentiated by aquifer and water type. SJR-r—San Juan del Río aquifer rain; SJR-sp—San Juan del Río aquifer spring; SJR-gw—San Juan del Río aquifer groundwater; Qro-gw—Querétaro aquifer groundwater; Cel-gw—Celaya aquifer groundwater; LG—El Geyser; LTGW—low-temperature groundwater; HTGW—high-temperature groundwater. (D) PCA diagram differentiated by aquifer cluster water type.

on the major Euclidean distance break in the amalgamation graph (Fig. 2A). The PCA illustrates the strong apparent correlation between water type and physicochemical parameters and confirms that our differentiation is robust. In Figures 2C and 2D, rain and low-temperature groundwater (LTGW; temperature <35 °C) share a geochemical evolution on a continuum. The internal division of LTGW suggests an east–west enrichment (from San Juan del Río to Celaya) in Ca^{2+}-Mg^{2+}-HCO_3^-, which is in good agreement with piezometric gradient and residence time/water-rock interaction processes. To simplify the data presentation and discussion, the rainwaters and LTGW (<35 °C) will be considered, respectively, as a single population (Figs. 2C and 2D). Three other populations are evident in Figure 2D: (1) the geothermal springs from Los Azufres, (2) El Geyser, and (3) the groundwater of anomalous temperature in the San Juan del Río–Querétaro–Celaya aquifers (temp >35 °C, high-temperature groundwater [HTGW], Fig. 2C; and <35 °C, Fig. 2D). It is remarkable that the Los Azufres and El Geyser geothermal springs represent two different end-members. The Geyser springs are characterized by high temperatures and Na^+-Cl^- and Fluor enrichment. HTGW samples seem to represent a mixing pattern from LTGW to the El Geyser end-members. Finally, few samples from Celaya aquifer compose the cluster 5. They are characterized by SO_4^{2-} and K^+ enrichment probably related to the dissolution of Jurassic evaporites. The special case of high-sulfate water in the PC gas sample is related to the observed precipitation of carbonate in the water deposit from where it was sampled. Cl^-–SO_4^{2-} water composition and increasing temperatures in all of the basins are correlated with specific geographic features (buried N–S faults), which indicates that the regional geology/lithology may be a determining factor that influences the physicochemical characteristics of water. The δ^2H-$\delta^{18}O$ isotopic composition of all rainwater, spring water, and groundwater (LTGW and HTGW; Fig. 3) is close to the Global Meteoric Water Line and Local Meteoric Water Line (LMWL) defined for San Juan del Río by Hernández-Pérez et al. (2020), which indicates a main meteoric contribution. All groundwater clusters (LMWL; Celaya, Querétaro, San Juan del Río aquifers) plot along common regression lines comparable to the Local Evaporation Line (LEL) as defined by Hernández-Pérez et al. (2020; LEL: $\delta^2H = 5.38\ \delta^{18}O - 19.84$). Even the HTGW samples from San Juan del Río–Celaya Valley (including geothermal fluids from El Geyser) do not show evidence of an andesitic source.

Evaluation of the physicochemical and isotopic data set from the San Juan del Río–Querétaro–Celaya groundwater (LTGW and HTGW) and springs, including El Geyser, shows no relationship to the Los Azufres samples or a volcanic water signature.

Gas Chemistry and Helium Isotopes

N_2, CO_2, and O_2 are the predominant dissolved gas species in the groundwater samples (Table 1). Their concentrations range from 8.12×10^{-3} to 1.1×10^{-2} cm³ STP/g for the N_2, 1.6×10^{-4} to 6.2×10^{-3} cm³ STP/g for the CO_2,

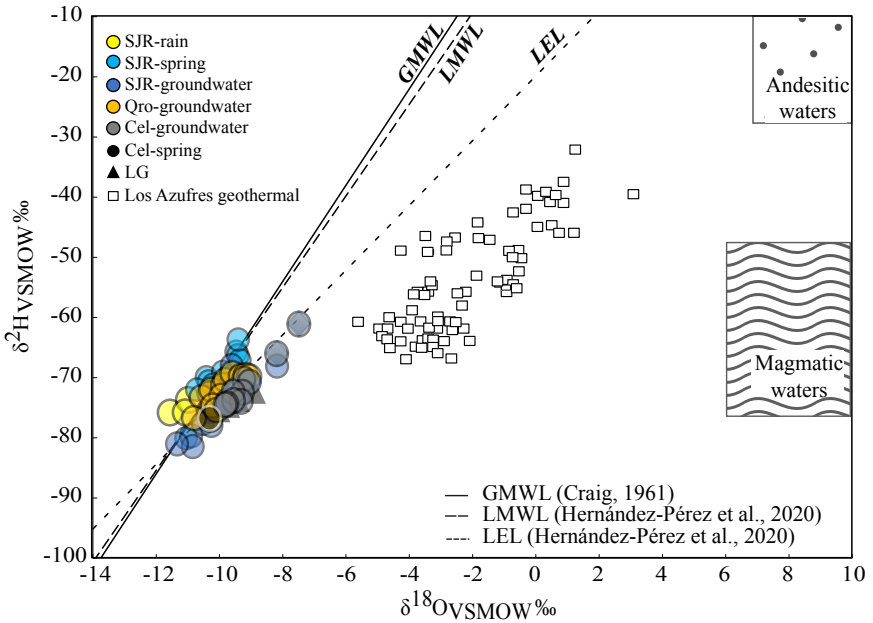

Figure 3. δ^2H–$\delta^{18}O$ isotopic data from groundwater samples (spring and wells) from the Celaya (Cel)–Querétaro (Qro)–San Juan del Río (SJR) basins show a main evaporation isotopic trend with a common meteoric origin (Hernández-Pérez et al., 2022; Amézaga-Campos et al., 2022). For comparison, the isotopic data from regional hydrothermal springs and wells were added (El Geyser and Los Azufres; Barragan et al., 2005; González-Partida et al., 2005; González-Guzmán et al., 2019; Pinti et al., 2013; Nieva et al., 1987). VSMOW—Vienna Standard Mean Ocean Water. GMWL—Global Meteoric Water Line; LMWL—Local Meteoric Water Line; LEL—Local Evaporation Line. LG is a sample.

TABLE 1. PHYSICAL COMPOSITION AND He-Ne-C ISOTOPIC COMPOSITION OF THE GROUNDWATER DISSOLVED GAS FRACTION OF THE CELAYA, QUERÉTARO, AND SAN JUAN DEL RÍO AQUIFERS

Sample type	Dissolved gases							Free gas
Sample name	Santa Cruz Forrajes (SCF)	El Lobo (EL)	Saldarraga (Sal)	La D (LD)	Amealco 1 (Ame)	Palmillas (Pal)	Pozo Celaya (PC) (water flow condensed steam deposit)	Pozo Geotérmico Celaya
Aquifer	Qro	Qro	Qro	SRJ	SRJ	SRJ	Cel	Cel
Long	363597	375555	365807	380114	382137	405328	317759	317759
Lat	2291117	2290015	2281668	2261430	2234320	2245940	2270992	2270992
T (°C)	42.7	41.4	39.7	34.5	20.7	41.6	87.9	–
pH	8.0	7.5	8.8	8.0	7.5	8.7	9.0	–
EC (µs/cm)	434	466	489	282	152	441	5920	–
TDS (ppm)	213	229	240	139	74	216	2905	–
ORP (mV)	14	21	3	54	24	213	–193	–
R/Ra (Laboratory)	0.36	2.96	2.67	0.99	0.85	1.30	–	2.31
$^{4}He/^{20}Ne$ (Laboratory)	1.94	2.17	11.99	0.35	0.34	6.06	–	150.36
Rc/Ra	0.25	3.25	2.71	–	–	1.31	–	2.31
$^{3}He/^{4}He$	3.49E-07	4.50E-06	3.75E-06	1.33E-06	2.73E-07	1.81E-06	–	3.20E-06
cm^3 STP/g for dissolved gas, ppm and % for free gas								
^{4}He (ppm)	4.19E-07	4.60E-07	2.54E-06	7.41E-08	7.12E-08	1.65E-06	–	121.55
H_2 (ppm)	<LoD	<LoD	<LoD	<LoD	<LoD	3.40031E-07	–	1406
N_2 (%)	9.08E-03	8.12E-03	1.10E-02	9.80E-03	1.03E-02	1.11E-02	–	4.74
O_2 (%)	1.46E-03	8.98E-04	7.24E-04	1.94E-03	1.13E-03	4.69E-04	–	1.21
CO (ppm)	<LoD	<LoD	<LoD	3.68E-08	3.60E-08	1.80E-07	–	<LoD
CH_4 (ppm)	6.06E-08	2.04E-06	4.03E-07	7.54E-08	6.57E-08	1.40E-06	–	1.9
CO_2 (%)	9.70E-04	5.50E-03	1.85E-04	1.67E-03	6.20E-03	1.60E-04	–	93.03
^{20}Ne (ppm)	2.13E-07	2.09E-07	2.10E-07	2.06E-07	2.06E-07	2.71E-07	–	0.81
Ar (ppm)	2.75E-04	4.61E-04	3.01E-04	4.04E-04	2.80E-04	3.18E-04	–	1174.01

Note: Dashes indicate not measured or not calculated data. <LoD indicates data under limit of detection.

and 4.69×10^{-4} to 1.94×10^{-3} cm^3 STP/g for the O_2. Groundwater samples have ^{4}He concentrations between 7.13×10^{-8} cm^3 STP/g and 2.54×10^{-6} cm^3 STP/g with Rc/Ra values ranging from 0.2 to 3.25 (Table 1). $^{4}He/^{20}Ne$ (Laboratory) isotopic ratios dissolved in waters vary from 0.34 to 11.9, all of which are above the air-saturated water (ASW) composition ratio of 0.288.

The free gas sample from the Celaya geothermal well (PC) has a composition dominated by 93% CO_2, 4.7% N_2, and 1.2% O_2, with a ^{4}He concentration of 122 ppm. The measured $^{4}He/^{20}Ne$ ratio is 150, with an Rc/Ra value of 2.31 (Table 1).

DISCUSSION

Volatile Composition of Groundwater

The relative proportions of CO_2, N_2, and O_2 of the San Juan del Río–Querétaro–Celaya dissolved and free gas samples and El Geyser bubbling gas samples were plotted in a triangular plot (Fig. 4A) and compared with the air and ASW values. Most of the dissolved gas samples are characterized by a CO_2 enrichment with respect to the ASW, evincing interaction with non-atmospheric CO_2. There is no clear relationship between this CO_2 enrichment and the Rc/Ra values (Fig. 4B). Samples Pal and Sal show an enrichment in N_2, which may be due to an interaction with Quaternary organic sediments filling the San Juan del Río graben, as these samples show a slight enrichment in CH_4 and the Pal sample also records CO concentration (Table 1).

The dry-gas chemical composition of the geothermal well in Celaya city (PC) is also characterized by a CO_2 enrichment with respect to the air composition, evincing interaction with non-atmospheric CO_2. Los Geysers bubbling gas samples display a mixing trend between air composition and a CO_2-dominated hydrothermal end-member. These samples have a relatively constant Rc/Ra value (mainly from 1.31 to 1.74; González-Guzmán et al., 2019) with variable proportions of CO_2 (Fig. 4B). This behavior, for such a small sampling area, implies different local mechanisms for the CO_2 enrichment dynamics. The $\delta^{13}C$ signatures of bubbling gas and groundwater at El Geyser can be explained as part of a mixing process with an organic end-member from the sedimentary rocks in the area (Marín-Camacho et al., 2022). On the other hand, the PC sample has the highest CO_2 concentration (93.03%), as well as the highest Rc/Ra value for free gas samples (2.31

Ra). Also, considering the helium isotopes in dissolved gases, the highest Rc/Ra value (3.25) was found in the EL sample (41.4 °C) in the San Juan del Río–Querétaro–Celaya area.

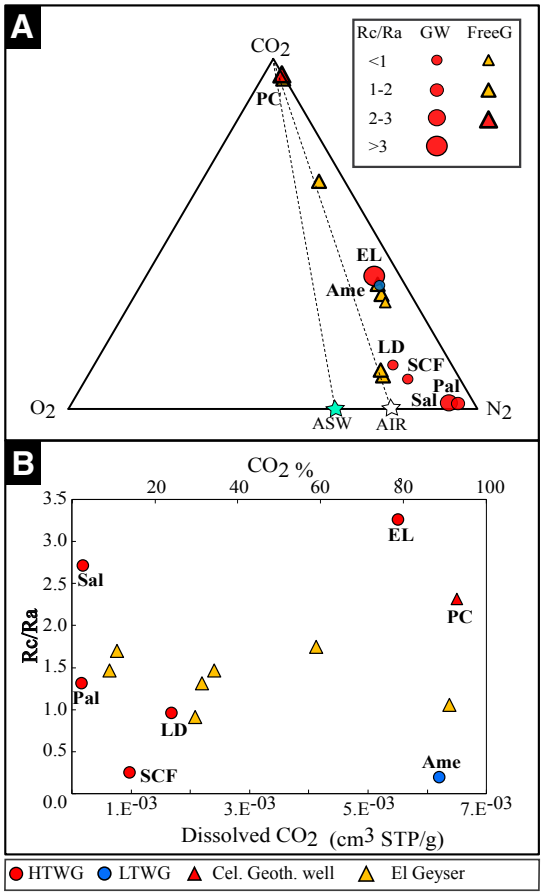

Figure 4. (A) CO_2-O_2-N_2 ternary diagram for the Celaya (Cel)–Querétaro (Qro)–San Juan del Río (SJR) groundwater samples is shown. The typical values of air (AIR) and air-saturated water (ASW) after O'Nions and Oxburgh (1988) and Smith and Kennedy (1983) are also plotted. GW—groundwater; FreeG—free gas. (B) Dissolved CO_2 (for low-temperature groundwater [LTGW] and high-temperature groundwater [HTGW] in cc/g) and free CO_2 (for the Celaya Geothermal Well and El Geyser in %) vs. Rc/Ra diagram for the Cel-Qro-SJR groundwater samples. Data from El Geyser geothermal area were taken from González-Guzmán et al. (2019). SCF, PC, Sal, EL, LD, Pal, and Ame are sample names.

Mantle-Helium Sources and Transport Mechanisms

Helium is an excellent geochemical proxy for distinguishing mantle and crustal contributions. Given the different origins, the ratio between primordial (^{3}He) and radiogenic (^{4}He) varies according to the tectonic setting. In the continental crust, radiogenic ^{4}He production dominates, exhibiting an average ^{3}He/^{4}He crust end-member ratio of 0.02 Ra (Hooker et al., 1985). On the contrary, regions with mantle-derived fluids such as volcanic arcs, and mid-oceanic ridges or regions with active faults and high-seismicity, can reach average mantle end-member ratios of ^{3}He/^{4}He (Gautheron and Moreira, 2002; Graham, 2002; Hilton et al., 2002; Kulongoski et al., 2005; Hilton, 2007; Kennedy and Van Soest, 2007; Hilton and Porcelli, 2014).

The R/Ra ratio versus the ^{4}He/^{20}Ne ratio for each sample is plotted in Figures 5A and 5B. The end-members, as well as the Los Azufres geothermal wells, springs, mud volcanoes, and fumarole samples (Pinti et al., 2013; Wen et al., 2018), were plotted for comparison. The mantle, atmospheric, and crustal helium contribution (Table 1, Figs. 5A and 5B) was calculated following the equation system proposed by Sano and Wakita (1985):

$$\frac{R}{R_a} = A\frac{R}{R_{a_{ASW}}} + M\frac{R}{R_{a_m}} + C\frac{R}{R_{a_c}} \quad (3)$$

$$\frac{1}{\frac{^4\text{He}}{^{20}\text{Ne}}} = \frac{A}{\frac{^4\text{He}}{^{20}\text{Ne}_{ASW}}} + \frac{M}{\frac{^4\text{He}}{^{20}\text{Ne}_m}} + \frac{C}{\frac{^4\text{He}}{^{20}\text{Ne}_c}} \quad (4)$$

$$A + M + C = 1 \quad (5)$$

where *A*, *M*, and *C* represent the atmospheric, mantle, and crustal He components, respectively. The end-members used for the calculations are ^{4}He/^{20}Ne ratios of 0.265 for ASW (Smith and Kennedy, 1983) or 0.318 for air (O'Nions and Oxburgh, 1988), and 1000 for crustal and mantle fluids (Craig et al., 1978; Sano and Wakita, 1985); and the R/Ra ratios of 0.983 Ra for ASW (Benson and Krause, 1980) or 1 Ra for air (Graham, 2002), 0.02 Ra for the crust (Hooker et al., 1985), and 7.3 Ra for the lithospheric mantle beneath Mexico (Straub et al., 2011).

Most of the dissolved gas samples have less than a 50% contribution from ASW (except for Ame and LD). The main He source is a variable mixture of the crustal (48–82%) and mantle end-members (2.7–39%). The mantle contribution is relatively high for groundwater in a typical continental crust without recent magmatism (Mamyrin and Tolstikhin, 1984). The bubbling gas samples from El Geyser have an important atmospheric contribution (3.4–60%), a crustal contribution varying from 36% to 76%, and a mantle proportion of 4–21%. The geothermal well (PC sample) has the least atmospheric contribution (0.2%), and a major crustal proportion (68.4%) but with a high percentage of mantle-derived helium (31.4%). The San Juan del Río–Querétaro–Celaya samples have a distinct proportion of crustal- and mantle-He unlike Los Azufres, which lies

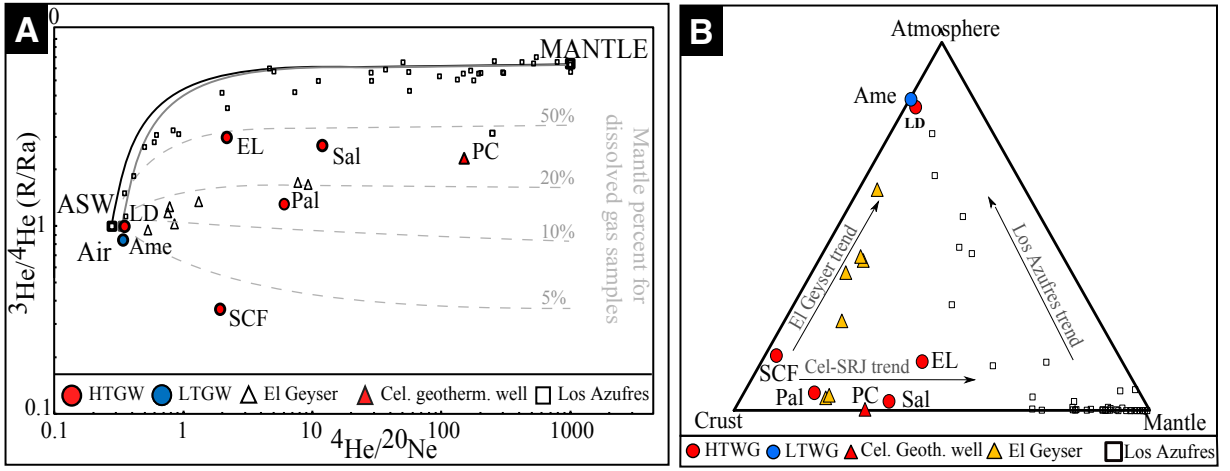

Figure 5. (A) Diagram shows $^3He/^4He$ vs. $^4He/^{20}Ne$ (after Sano and Wakita, 1985) for dissolved and free gas samples from Celaya (Cel)–Querétaro (Qro)–San Juan del Río (SJR) aquifers and Los Azufres geothermal field. Air (air) and ASW (air-saturated water) denote the atmospheric end-members (the first for the free gas and the second for the dissolved gas). The solid lines show the mixture of the atmospheric end-members with mantle end-members. The $^4He/^{20}Ne$ end-member ratios used are 0.265 for air and ASW (Smith and Kennedy, 1983) and 1000 for crustal and mantellic fluids (Sano and Wakita, 1985). The R/Ra end-member ratios used are 1 Ra for Air, 0.983 Ra for ASW (Benson and Krause, 1980), 0.02 Ra for the crust (Hooker et al., 1985), and 7.3 Ra for the lithospheric mantle in Mexico (Straub et al., 2011). Data from Los Azufres were taken from Pinti et al. (2013) and Wen et al. (2018). Data from El Geyser were taken from González-Guzmán et al. (2019). HTGW—high-temperature groundwater; LTGW—low-temperature groundwater. No error bars are shown because they are similar to or smaller than the symbol size. Solid gray and black lines are the mixing curves between the air and mantle and the ASW and mantle end-members, respectively. (B) Atmosphere–crust–mantle ternary diagram. Santa Cruz Forajes (SCF), Saldarraga (Sal), El Lobo (EL), La D (LD), Palmillas (Pal), Amealco (Ame), and Celaya Geothermal Well (PC) are sample names.

in a typical volcanic setting in the Trans-Mexican Volcanic Belt (Figs. 1B and 4B). Helium isotopes from Los Azufres springs and geothermal wells (Pinti et al., 2013), which are considered here for comparison, are characterized by an almost binary mixture that is between those of the atmospheric and mantellic end-members. These results imply a different tectonic-structural framework.

The geographical distribution of samples in the San Juan del Río–Querétaro–Celaya region may shed some light on the ^3He enrichment mechanism in groundwater. In the Celaya-Querétaro region, the El Geyser bubbling springs lie on the Obrajuelo N–S fault trace, and the PC geothermal well is also inferred to be located above a buried N–S fault (Fig. 1C). In Querétaro–San Juan del Río, sample LD is close to Sanfandila, a town where a seismic swarm took place in 1998 (Zúñiga et al., 2003); the Sal sample also lies close to the inferred Sanfandila fault trace, while EL lies within the intersection of the NW–SE and the NE–SW faults systems, at the rim of the Amazcala caldera (ca. 7.3 Ma; Fig. 1C). There is a clear relationship between the location of the thermally high Rc/Ra samples and the structural setting of the region, which implies that faults transport ^3He toward the surface, although the origin of this ^3He is not obvious.

We tested two hypotheses to assess a possible origin for the high Rc/Ra values within an intra-arc extension environment: (1) ^3He enrichment due to a volatile-rich magma aging at depth (crust building by magma injection), and (2) ascent of volatiles degassed from mantle melts enhanced by crustal permeability in proximity to the regional fault systems coupled with crustal extension (Kennedy and van Soest, 2006).

Remnant Magmatic Fluids/Magma Aging Model

The magma aging model, first proposed by Torgersen and Jenkins (1982) and further developed by Kennedy and van Soest (2006) and Méjean et al. (2020), was used to test the first hypothesis. The magma aging model considers that in the absence of a present degassing magmatic source in the crust, anomalously high ^3He contribution sources could derive from the leaching of local magmatic rocks rich in ^3He trapped in the rocks (Torgersen and Jenkins, 1982; Méjean et al., 2020). To distinguish if this ^3He signature comes from the local magmatic rocks, we calculated the present-day helium composition that might be found according to their ages. In the crust, the time-dependent change in the helium isotopic composition of a reservoir due to the addition of radiogenic ^4He is described by the equation (Newell et al., 2015):

$$\left(\frac{^3He}{^4He}\right)_{fin} = \frac{\left(^3He\right)_{init}}{\left(^4He_{init} + {}^4He_{rad} \times t\right)} \quad (6)$$

where *fin* and *init* refer to the final (present-day) and initial concentrations (cm^3STP/g) or ratios, it is the time since the magmatic event/emplacement (yr), and $^4He_{rad}$ is the accumulation rate of radiogenic helium in the fluid ($cm^3STP/g/yr$) given by:

$$^4He_{rad} = {}^4He_{prod} \times \frac{(1-\varphi)}{\varphi} \quad (7)$$

where φ is the porosity, and $^4He_{prod}$ is the crustal production rate ($cm^3STP/g/yr$), which can be calculated following the equation (Torgersen et al., 1995):

$$^4He_{prod} = \left(0.2355 \times 10^{-12}\right) \times [U] \times \left(1 + 0.123\left(\frac{[Th]}{[U]} - 4\right)\right) \quad (8)$$

where $[U]$ and $[Th]$ are the concentrations of U and Th in the rock in ppm. In absence of local representative data, we used the $[U]$ and $[Th]$ concentrations of an average continental upper crust (2.7 ppm and 10.5 ppm, respectively; Rudnick and Gao, 2003).

In agreement with the regional geology, we considered two possible sources for a rich mantellic helium: the latest volcanism in the San Juan del Río–Querétaro–Celaya area, which corresponds to the Amazcala, Amealco and Huichapan calderas (ca. 7.3–3.0 Ma; Aguirre-Díaz and López-Martínez, 2001), and the monogenetic volcanism of the Michoacán-Guanajuato volcanic field (average 300–400 ka; Gómez-Vasconcelos et al., 2020). We calculated the remaining $^3He/^4He$ ratio of the magmatic fluid without considering mixing processes using the ages of these two volcanic events. According to the helium concentration measured in olivine from the Pleistocene to present Trans-Mexican Volcanic Belt (Straub et al., 2011), we assume a $^4He_{init}$ value of 2.84×10^{-8} cm^3STP/g, and a $^3He_{init}$ value of 2.87×10^{-13} cm^3STP/g for the lithospheric mantle in central Mexico. Considering that these magmatic rocks are emplaced or can interact with water within the upper crust, we used a $^4He_{prod}$ value of 6.27×10^{-13} $cm^3STP/g/y$. For the porosity value, we used 10% as an average in a fractured sedimentary and volcaniclastic upper crust (Carrera-Hernández et al., 2016; Alaniz-Álvarez et al., 2001).

Results using the youngest caldera's event (ca. 3.0 Ma) yield a remaining $^3He/^4He$ ratio of 1.69×10^{-8} (0.01 Ra), while the monogenetic volcanism (300 ka) yields a remaining $^3He/^4He$ ratio of 1.67×10^{-7} (0.12 Ra). The values calculated represent a maximum, as we are not considering mixing or dilution within the aquifers. Calderas (ca. 3 Ma) or monogenetic volcanic (<300 ka) sources in the upper crust for the high mantle He contribution seem unlikely. In both cases, the predicted helium composition in the remaining fluid is several orders of magnitude lower than the range of Rc/Ra ratios measured in the study area. To reach Rc/Ra values as high as 3.25, such as those measured in the EL sample, and without considering aquifer dilution, the age of the magma source should be less than 6 ka. But such young magmatism is absent in the study region.

Sublithospheric Mantle He Flow through the Crust

To better asses the origin of the mantellic helium source, we estimated a travel-time range for the helium coming from the sublithospheric mantle to the surface using equations 6, 7, and 8. In this case, $^4He_{prod} = 2.59 \times 10^{-14}$ $cm^3STP/g/yr$ was calculated using concentrations of U and Th in average mid-oceanic-ridge basalt (0.119 and 0.4, respectively; Gale et al., 2013) as a proxy for the composition of the subcontinental lithospheric mantle beneath Mexico. The $(3He/4He)_{fin}$ values used were the ratios measured in San Juan del Río–Querétaro–Celaya samples, except for the Ame cold-shallow aquifer sample. The $^4He_{init}$ and $^3He_{init}$ values used remained the same (2.84×10^{-8} and 2.87×10^{-13} cm^3STP/g, respectively; Straub et al., 2011). We considered an average crustal thickness of 40 km (Urrutia-Fucugauchi and Flores-Ruiz, 1996). As for the porosity, we used a value of φ = 1% as an upper limit for the lower crust (Hiett et al., 2021). Using Equation 7, we obtained He residence times of 14–300 k.y. (with an average of 80 k.y.). These residence times can be used to calculate an He flow rate. Considering a 40-km-thick crust, we have flow rates of 0.1–2.9 m/yr. Calculated ^3He flow rates are comparable to the flow rates from other active crustal fault zones such as the San Andreas fault (0.004–0.14 m/yr; Kennedy et al., 1997; Kulongoski et al., 2013), the North Anatolian fault (0.13–0.19 m/yr; de Leeuw et al., 2010), the Karakoram fault (0.012–0.019 m/yr; Klemperer et al., 2013), and the Alpine fault (0.42–2.6 m/yr; Menzies et al., 2016). Although these calculations are an approximation for the extent and rate of degassing in the San Juan del Río–Querétaro–Celaya area, they are comparable to the estimates for other regions where the mantle degassing is controlled by major crustal fault systems.

Regional Implications

The residence times calculated suggest that the partial melting event in the subcontinental sublithospheric mantle could be part of the event that created the Michoacán-Guanajuato volcanic field. The distribution of this monogenetic volcanism is strongly controlled by pre-existing, ~N–S-trending, and locally still active fault systems (Gómez-Vasconcelos et al., 2020). Although the high ^3He points to partial melting in the mantle, according to our re-evaluation of the hydrogeologic system and the dissolved gas data, there is no evidence of magmatic activity in the same range of time (< 300 k.y.).

In our study area, the distribution of the mantellic helium in the San Juan del Río–Querétaro–Celaya aquifers is strongly controlled by the permeability associated with the N–S systems of the fault. The extent of ^3He degassing seems to be different in the aquifers; for example, ^3He flow rates are higher for the dissolved gas samples in the San Juan del Río–Querétaro aquifers than for those in the Celaya aquifer (El Geyser and PC). For instance, the EL and Sal samples (from 200–300-m-deep wells, with temperatures of ~40 °C) have higher mantle helium flux than the PC sample from a 2500-m-deep geothermal production well. In general, toward the west of the San Miguel Allende–Taxco fault system, we find high-enthalpy waters (Celaya) but with a moderate mantle

helium contribution, while to the east of the San Miguel Allende–Taxco fault system, we find the thermal anomalies associated with a high input of mantle helium. The eastern portion of the San Juan del Río–Querétaro–Celaya area seems to be more permeable, which could also be related to the seismic activity in the region (Zúñiga et al., 2003; Aguirre-Díaz et al., 2005).

CONCLUSIONS

The hydrochemical and helium isotopic compositions in the study area provide insights into the dynamics of volatile degassing in the northern part of the central Trans-Mexican Volcanic Belt. The San Juan del Río–Querétaro–Celaya area, located within the intersection of two regional fault systems, contains thermal waters with a high input of ^{3}He. The water has a meteoric origin and is not influenced by volcanic water or gas, as in other geothermal areas of the Trans-Mexican Volcanic Belt, such as Los Azufres, which is located ~70 km to the south. The high contribution of ^{3}He is related to the partial melting of the sublithospheric mantle, and the ascent of this mantle helium from the base of the crust to the surface is controlled by the San Miguel Allende–Taxco and Chapala-Tula regional fault systems.

Our results emphasize the importance of regional crustal fault systems as important pathways for volatile degassing in the Trans-Mexican Volcanic Belt in addition to the large volcanic centers. Additional geophysical data on the structure of the upper mantle to the north of the central Trans-Mexican Volcanic Belt, coupled with a better knowledge of the stress regime in the crust, will help to confirm the mechanism that leads to the active volatile degassing without magmatic activity observed in central Mexico.

ACKNOWLEDGMENTS

This research is part of A. Billarent-Cedillo's Master of Science project in the framework of the Universidad Nacional Autónoma de Mexico (UNAM) postgraduate program. The research was funded by CONACYT grant CB-255070 to G. Levresse, and by the UNAM-DGAPA PAPIIT grant IV100117 (Centro de Geociencias and Facultad the Ingeniería, Hydrogeology Group, UNAM). We thank Comité Técnico de Aguas Subterráneas de San Juan del Río, and Comisión Estatal de Aguas Querétaro for sharing information and logistical support. The manuscript benefited greatly from the reviews of Daniele L. Pinti and an anonymous reviewer.

REFERENCES CITED

Aguirre-Díaz, G.J., 1996, Volcanic stratigraphy of the Amealco caldera and vicinity, Central Mexican Volcanic Belt: Revista Mexicana de Ciencias Geológicas, v. 13, p. 10–51.

Aguirre-Díaz, G.J., and López-Martínez, M., 2001, The Amazcala caldera, Querétaro, Mexico. Geology and geochronology: Journal of Volcanology and Geothermal Research, v. 111, p. 203–218, https://doi.org/10.1016/S0377-0273(01)00227-X.

Aguirre-Díaz, G.J., and López-Martínez, M., 2009, Geologic evolution of the Donguinyó-Huichapan caldera complex, central Mexican Volcanic Belt, Mexico: Journal of Volcanology and Geothermal Research, v. 179, p. 133–148, https://doi.org/10.1016/j.jvolgeores.2008.10.013.

Aguirre-Díaz, G.J., and McDowell, F.W., 2000, Volcanic evolution of the Amealco caldera, central Mexico, *in* Delgado-Granados, H., Aguirre-Díaz, G.J., and Stock, J.M., eds., Cenozoic Tectonics and Volcanism of Mexico: Geological Society of America Special Paper 334, p. 179–193, https://doi.org/10.1130/0-8137-2334-5.179.

Aguirre-Díaz, G.J., Nieto-Obregón, J., and Zúñiga, F.R., 2005, Seismogenic basin and range and intra-arc normal faulting in the central Mexican Volcanic Belt, Querétaro, México: Geological Journal, v. 40, p. 215–243, https://doi.org/10.1002/gj.1004.

Alaniz-Álvarez, S.A., and Nieto-Samaniego, Á.F., 2005, El sistema de fallas Taxco–San Miguel de Allende y la Faja Volcánica Transmexicana, dos fronteras tectónicas del centro de México activas durante el Cenozoico: Boletín de la Sociedad Geológica Mexicana, v. 57, p. 65–82, https://doi.org/10.18268/BSGM2005v57n1a4.

Alaniz-Álvarez, S.A., Nieto-Samaniego, Á.F., Reyes-Zaragoza, M.A., Orozco-Esquivel, M.T., Ojeda-García, Á.C., and Vassallo, L.F., 2001, Estratigrafía y deformación extensional en la región San Miguel de Allende-Querétaro, México: Revista Mexicana de Ciencias Geológicas, v. 18, p. 129–148.

Alaniz-Álvarez, S.A., Nieto-Samaniego, A.F., Orozco-Esquivel, M.T., Vassallo, L.F., and Xu, S., 2002, El sistema de fallas Taxco-San Miguel de Allende: Implicaciones en la deformación post-eocénica del centro de México: Boletín de la Sociedad Geológica Mexicana, v. 55, p. 12–29, https://doi.org/10.18268/BSGM2002v55n1a2.

Amézaga-Campos, B.S., Villanueva-Estrada, R., Carrillo-Chavez, A., Morales-Arredondo, J.I., and Morán-Ramírez, J., 2022, Hydrogeochemistry characterization of an overexploited municipal, agricultural, and industrial aquifer, central Mexico: Applied Geochemistry, v. 142, https://doi.org/10.1016/j.apgeochem.2022.105310.

Aranda-Gómez, J.J., and McDowell, F.W., 1998, Paleogene extension in the southern basin and range province of Mexico: Syndepositional tilting of Eocene red beds and Oligocene volcanic rocks in the Guanajuato mining district: International Geology Review, v. 40, p. 116–134, https://doi.org/10.1080/00206819809465201.

Arango-Guevara, A.F., Mitre-Salazar, L.M., and Martínez-Reyes, J., 2007, Actualización del conocimiento geológico en la Cuenca del Río Chichimequillas, Estado de Querétaro, México ANDRÉS: Trabajos de Geología 27, Universidad de Oviedo, p. 29–39.

Arce, J.L., Rangel, E., Valdez-Moreno, G., Saucedo, R., Castro-Govea, R., and Macías, J.L., 2021, Caracterización geoquímica, petrográfica y evolucion magmática del Campo Volcánico de Los Azufres, Michoacan, durante el Pleistoceno: Revista Mexicana de Ciencias Geológicas, v. 38, p. 122–140; https://doi.org/10.22201/cgeo.20072902e.2021.2.1646.

Ballentine, C.J., and Burnard, P.G., 2002, Production, release and transport of noble gases in the continental crust: Reviews in Mineralogy and Geochemistry, v. 47, p. 481–538, https://doi.org/10.2138/rmg.2002.47.12.

Ballentine, C.J., Marty, B., Lollar, B.S., and Cassidy, M., 2005, Neon isotopes constrain convection and volatile origin in the Earth's mantle: Nature, v. 433, p. 33–38, https://doi.org/10.1038/nature03182.

Barragán, R.M., Arellano, V.M., Portugal, E., and Sandoval, F., 2005, Isotopic ($\delta^{18}O$, δD) patterns in Los Azufres (México) geothermal fluids related to reservoir exploitation: Geothermics, v. 34, p. 527–547.

Bekaert, D.V., Turner, S.J., Broadley, M.W., Barnes, J.D., Halldoacutersson, S.A., Labidi, J., Wade, J., Walowski, K.J., and Barry, P.H., 2021, Subduction-driven volatile recycling: A global mass balance: Annual Review of Earth and Planetary Sciences, v. 49, p. 37–70, https://doi.org/10.1146/annurev-earth-071620-055024.

Benson, B.B., and Krause, D., 1980, Isotopic fractionation of helium during solution: A probe for the liquid state: Journal of Solution Chemistry, v. 9, p. 895–909, https://doi.org/10.1007/BF00646402.

Botero-Santa, P.A., Alaniz-Álvarez, S.A., Nieto-Samaniego, Á.F., López-Martínez, M., Levresse, G., Xu, S., and Ortega-Obregón, C., 2015, Origen y desarrollo de la cuenca El Bajío en el sector central de la faja Volcánica Transmexicana: Revista Mexicana de Ciencias Geológicas, v. 32, p. 84–98.

Buttitta, D., Caracausi, A., Chiaraluce, L., Favara, R., Gasparo Morticelli, M., and Sulli, A., 2020, Continental degassing of helium in an active tectonic setting (northern Italy): The role of seismicity: Scientific Reports, v. 10, p. 1–13, https://doi.org/10.1038/s41598-019-55678-7.

Byerlee, J., 1993, Model for episodic flow of high-pressure water in fault zones before earthquakes: Geology, v. 21, p. 303–306, https://doi.org/10.1130/0091-7613(1993)021<0303:MFEFOH>2.3.CO;2.

Capasso, G., and Inguaggiato, S., 1998, A simple method for the determination of dissolved gases in natural waters. An application to thermal waters from Vulcano Island: Applied Geochemistry, v. 13, p. 631–642, https://doi.org/10.1016/S0883-2927(97)00109-1.

Carrera-Hernández, J.J., Carreón-Freyre, D., Cerca-Martínez, M., and Levresse, G., 2016, Groundwater flow in a transboundary fault-dominated aquifer and the importance of regional modeling: The case of the city of Querétaro, Mexico: Hydrogeology Journal, v. 24, p. 373–393, https://doi.org/10.1007/s10040-015-1363-x.

Craig, H., Lupton, J.E., Welhan, J.A., and Poreda, R., 1978, Helium isotope ratios in Yellowstone and Lassen Park volcanic gases: Geophysical Research Letters, v. 5, p. 897–900, https://doi.org/10.1029/GL005i011p00897.

Dávalos-Álvarez, O.G., Nieto-Samaniego, Á.F., Alaniz-Álvarez, S.A., and Gómez-González, J.M., 2005, Las fases de deformación cenozoica en la región de Huimilpan, Querétaro, y su relación con la sismicidad local: Revista Mexicana de Ciencias Geológicas, v. 22, p. 129–147.

de Leeuw, G.A.M., Hilton, D.R., Güleç, N., and Mutlu, H., 2010, Regional and temporal variations in CO_2/^{3}He, ^{3}He/^{4}He and δ^{13}C along the North Anatolian Fault Zone, Turkey: Applied Geochemistry, v. 25, p. 524–539, https://doi.org/10.1016/j.apgeochem.2010.01.010.

Del Pilar-Martínez, A., Nieto-Samaniego, A.F., Alaniz-Alvarez, S.A., and Angeles-Moreno, E., 2020, Geology of the southern Mesa Central of Mexico: Recording the beginning of a polymodal fault system: Journal of Maps, v. 16, p. 199–211, https://doi.org/10.1080/17445647.2020.1719911.

Ferrari, L., Garduño, V.H., Pasquarè, G., and Tibaldi, A., 1991, Geology of Los Azufres caldera, Mexico, and its relationships with regional tectonics: Journal of Volcanology and Geothermal Research, v. 47, p. 129–148, https://doi.org/10.1016/0377-0273(91)90105-9.

Ferrari, L., Orozco-Esquivel, T., Manea, V., and Manea, M., 2012, The dynamic history of the Trans-Mexican Volcanic Belt and the Mexico subduction zone: Tectonophysics, v. 522–523, p. 122–149, https://doi.org/10.1016/j.tecto.2011.09.018.

Ferrari, L., Orozco-Esquivel, T., Bryan, S.E., López-Martínez, M., and Silva-Fragoso, A., 2018, Cenozoic magmatism and extension in western Mexico: Linking the Sierra Madre Occidental silicic large igneous province and the Comondú Group with the Gulf of California rift: Earth-Science Reviews, v. 183, p. 115–152, https://doi.org/10.1016/j.earscirev.2017.04.006.

Fitz-Díaz, E., Lawton, T.F., Juárez-Arriaga, E., and Chávez-Cabello, G., 2018, The Cretaceous–Paleogene Mexican orogen: Structure, basin development, magmatism and tectonics: Earth-Science Reviews, v. 183, p. 56–84, https://doi.org/10.1016/j.earscirev.2017.03.002.

Gale, A., Dalton, C.A., Langmuir, C.H., Su, Y., and Schilling, J.G., 2013, The mean composition of ocean ridge basalts: Geochemistry, Geophysics, Geosystems, v. 14, p. 489–518, https://doi.org/10.1029/2012GC004334.

Gautheron, C., and Moreira, M., 2002, Helium signature of the subcontinental lithospheric mantle: Earth and Planetary Science Letters, v. 199, p. 39–47, https://doi.org/10.1016/S0012-821X(02)00563-0.

Giggenbach, W.F., Sano, Y., and Wakita, H., 1993, Isotopic composition of helium, and CO_2 and CH_4 contents in gases produced along the New Zealand part of a convergent plate boundary: Geochimica et Cosmochimica Acta, v. 57, p. 3427–3455, https://doi.org/10.1016/0016-7037(93)90549-C.

Gómez-Tuena, A., Orozco-Esquivel, M.T., and Ferrari, L., 2005, Petrogénesis ígnea de la Faja Volcánica Transmexicana: Boletín de la Sociedad Geológica Mexicana, v. 3, p. 227–283, http://www.scielo.org.mx/pdf/bsgm/v57n3/1405-3322-bsgm-57-03-227-s1.pdf%0A, http://www.geociencias.unam.mx/~alaniz/SGM/Centenario/57-3/(2)Gomez.pdf.

Gómez-Vasconcelos, M.G., Macías, J.L., Ramón Avellán, D.R., Sosa-Ceballos, G., Garduño-Monroy, V.H., Cisneros-Máximo, G., Layer, P.W., Benowitz, J., López-Loera, H., Mendiola López, F.M., and Perton, M., 2020, The control of preexisting faults on the distribution, morphology, and volume of monogenetic volcanism in the Michoacán-Guanajuato Volcanic Field: Geological Society of America Bulletin, v. 132, p. 2455–2474, https://doi.org/10.1130/B35397.1.

González-Guzmán, R., Inguaggiato, C., Peiffer, L., Weber, B., and Kretzschmar, T., 2019, Fault-controlled geothermal fluids of the northern Trans-Mexican Volcanic Belt: A geochemical and isotopic study of the Los Geysers field (Valley of Querétaro, Mexico): Journal of Volcanology and Geothermal Research, v. 388, https://doi.org/10.1016/j.jvolgeores.2019.106681.

González-Partida, E., Carrillo-Chávez, A., Levresse, G., Tello-Hinojosa, E., Venegas-Salgado, S., Ramirez-Silva, G., Pal-Verma, M., Tritlla, J., and Camprubi, A., 2005, Hydro-geochemical and isotopic fluid evolution of the Los Azufres geothermal field, Central Mexico: Applied Geochemistry, v. 20, p. 23–39, https://doi.org/10.1016/j.apgeochem.2004.07.006.

Graham, D.W., 2002, Noble gas isotope geochemistry of mid-ocean ridge and ocean island basalts: Characterization of mantle source reservoirs: Reviews in Mineralogy and Geochemistry, v. 47, p. 247–317, https://doi.org/10.2138/rmg.2002.47.8.

Hasenaka, T., 1994, Size, distribution, and magma output rate for shield volcanoes of the Michoacán-Guanajuato volcanic field, Central Mexico: Journal of Volcanology and Geothermal Research, v. 63, p. 13–31, https://doi.org/10.1016/0377-0273(94)90016-7.

Hasenaka, T., and Carmichael, I.S.E., 1985, The cinder cones of Michoacán-Guanajuato, central Mexico: Their age, volume and distribution, and magma discharge rate: Journal of Volcanology and Geothermal Research, v. 25, p. 105–124, https://doi.org/10.1016/0377-0273(85)90007-1.

Hernández-Pérez, E., Levresse, G., Carrera-Hernández, J., and García-Martínez, R., 2020, Short term evaporation estimation in a natural semiarid environment: New perspective of the Craig–Gordon isotopic model: Journal of Hydrology, v. 587, https://doi.org/10.1016/j.jhydrol.2020.124926.

Hernández-Pérez, E., Levresse, G., Carrera-Hernandez, J., Inguaggiato, C., Vega-González, M., Corbo-Camargo, F., Carreón-Freyre, D.C., Billarent-Cedillo, A., Contreras, F.J.S., and Hernández, C.P.R., 2022, Geochemical and isotopic multi-tracing (δ^{18}O, δ^2H, δ^{13}C, Δ^{14}C) of groundwater flow dynamics and mixing patterns in the volcanoclastic aquifer of the semiarid San Juan del Río Basin in central Mexico: Hydrogeology Journal, v. 30, p. 2073–2095.

Hiett, C.D., Newell, D.L., and Jessup, M.J., 2021, ^{3}He evidence for fluid transfer and continental hydration above a flat slab: Earth and Planetary Science Letters, v. 556, https://doi.org/10.1016/j.epsl.2020.116722.

Hilton, D.R., 1996, The helium and carbon isotope systematics of a continental geothermal system: Results from monitoring studies at Long Valley caldera (California, U.S.A.): Chemical Geology, v. 127, p. 269–295, https://doi.org/10.1016/0009-2541(95)00134-4.

Hilton, D.R., 2007, Geochemistry: The leaking mantle: Science, v. 318, p. 1389–1390, https://doi.org/10.1126/science.1151983.

Hilton, D.R., and Porcelli, D., 2014, 3.7—Noble gases as mantle tracers, *in* Holland, H.D., and Turekian, K.K., eds., Treatise on Geochemistry (2nd edition), Volume 3: Amsterdam, Elsevier, p. 293–325, https://doi.org/10.1016/B978-0-08-095975-7.00217-5.

Hilton, D.R., Fischer, T.P., and Marry, B., 2002, Noble gases and volatile recycling at subduction zones: Reviews in Mineralogy and Geochemistry, v. 47, p. 319–370, https://doi.org/10.2138/rmg.2002.47.9.

Hooker, P.J., Bertrami, R., Lombardi, S., O'Nions, R.K., and Oxburgh, E.R., 1985, Helium-3 anomalies and crust-mantle interaction in Italy: Geochimica et Cosmochimica Acta, v. 49, p. 2505–2513, https://doi.org/10.1016/0016-7037(85)90118-8.

Husker, A., and Davis, P.M., 2009, Tomography and thermal state of the Cocos Plate subduction beneath Mexico City: Journal of Geophysical Research: Solid Earth, v. 114, https://doi.org/10.1029/2008JB006039.

Inguaggiato, S., and Rizzo, A., 2004, Dissolved helium isotope ratios in ground-waters: A new technique based on gas-water re-equilibration and its application to Stromboli volcanic system: Applied Geochemistry, v. 19, p. 665–673, https://doi.org/10.1016/j.apgeochem.2003.10.009.

Jácome-Paz, M.P., 2019, Two new geothermal prospects in the Mexican Volcanic Belt: La Escalera and Agua Caliente–Tzitzio geothermal springs, Michoacán, México: Geothermics, v. 80, p. 44–55, https://doi.org/10.1016/j.geothermics.2019.02.004.

Kennedy, B.M., and van Soest, M.C., 2006, A helium isotope perspective on the Dixie Valley, Nevada, hydrothermal system: Geothermics, v. 35, p. 26–43, https://doi.org/10.1016/j.geothermics.2005.09.004.

Kennedy, B.M., and van Soest, M.C., 2007, Flow of mantle fluids through the ductile lower crust: Helium isotope trends: Science, v. 318, p. 1433–1436, https://doi.org/10.1126/science.1147537.

Kennedy, B.M., Kharaka, Y.K., Evans, W.C., Ellwood, A., DePaolo, D.J., Thordsen, J., Ambats, G., and Mariner, R.H., 1997, Mantle fluids in the San Andreas Fault system, California: Science, v. 278, p. 1278–1281, https://doi.org/10.1126/science.278.5341.1278.

Kim, Y., Clayton, R.W., and Jackson, J.M., 2010, Geometry and seismic properties of the subducting Cocos Plate in central Mexico: Journal of Geophysical Research: Solid Earth, v. 115, B06310, https://doi.org/10.1029/2009JB006942.

Klemperer, S.L., Kennedy, B.M., Sastry, S.R., Makovsky, Y., Harinarayana, T., and Leech, M.L., 2013, Mantle fluids in the Karakoram Fault: Helium isotope evidence: Earth and Planetary Science Letters, v. 366, p. 59–70, https://doi.org/10.1016/j.epsl.2013.01.013.

Kulongoski, J.T., Hilton, D.R., and Izbicki, J.A., 2005, Source and movement of helium in the eastern Morongo groundwater basin: The influence of regional tectonics on crustal and mantle helium fluxes: Geochimica et Cosmochimica Acta, v. 69, p. 3857–3872, https://doi.org/10.1016/j.gca.2005.03.001.

Kulongoski, J.T., Hilton, D.R., Barry, P.H., Esser, B.K., Hillegonds, D., and Belitz, K., 2013, Volatile fluxes through the Big Bend section of the San Andreas Fault, California: Helium and carbon-dioxide systematics: Chemical Geology, v. 339, p. 92–102, https://doi.org/10.1016/j.chemgeo.2012.09.007.

López-Alvis, J., Carrera-Hernández, J.J., Levresse, G., and Nieto-Samaniego, Á.F., 2019, Assessment of groundwater depletion caused by excessive extraction through groundwater flow modeling: The Celaya aquifer in central Mexico: Environmental Earth Sciences, v. 78, p. 1–22, https://doi.org/10.1007/s12665-019-8497-4.

Luhr, J.F., Kimberly, P., Siebert, L., Jorge Aranda-Gómez, J., Housh, T.B., and Mattietti, G.K., 2006, México's Quaternary volcanic rocks: Insights from the MEXPET petrological and geochemical database, *in* Siebe, C., MarcíasGerardo, J.L., and Aguirre-Díaz, J., eds., Neogene–Quarternary Continental Margin Volcanism: A Perspective from México: Geological Society of America Special Paper 402, p. 1–44, https://doi.org/10.1130/2006.2402(01).

Mamyrin, B.A., and Tolstikhin, I.N., eds., 1984, Helium Isotopes in Nature: Developments in Geochemistry: Amsterdam, Elsevier, v. 3, 273 p., https://doi.org/10.1016/B978-0-444-42180-7.50003-X.
Marín-Camacho, P., Velasco-Tapia, F., Bernard-Romero, R., Weber, B., and González-Guzmán, R., 2022, New geochemical evidence constraining the water-rock-gas interaction on geothermal fluids of the Querétaro Graben, northern Trans-Mexican Volcanic Belt: Journal of South American Earth Sciences, v. 114, https://doi.org/10.1016/j.jsames.2021.103702.
Méjean, P., Pinti, D.L., Kagoshima, T., Roulleau, E., Demarets, L., Poirier, A., Takahata, N., Sano, Y., and Larocque, M., 2020, Mantle helium in Southern Quebec groundwater: A possible fossil record of the New England hotspot: Earth and Planetary Science Letters, v. 545, https://doi.org/10.1016/j.epsl.2020.116352.
Menzies, C.D., Teagle, D.A.H., Niedermann, S., Cox, S.C., Craw, D., Zimmer, M., Cooper, M.J., and Erzinger, J., 2016, The fluid budget of a continental plate boundary fault: Quantification from the Alpine Fault, New Zealand: Earth and Planetary Science Letters, v. 445, p. 125–135, https://doi.org/10.1016/j.epsl.2016.03.046.
Newell, D.L., Jessup, M.J., Hilton, D.R., Shaw, C.A., and Hughes, C.A., 2015, Mantle-derived helium in hot springs of the Cordillera Blanca, Peru: Implications for mantle-to-crust fluid transfer in a flat-slab subduction setting: Chemical Geology, v. 417, p. 200–209, https://doi.org/10.1016/j.chemgeo.2015.10.003.
Nieto-Samaniego, Á.F., Ferrari, L., Alaniz-Alvarez, S.A., Labarthe-Hernández, G., and Rosas-Elguera, J., 1999, Variation of Cenozoic extension and volcanism across the southern Sierra Madre Occidental volcanic province, Mexico: Geological Society of America Bulletin, v. 111, p. 347–363, https://doi.org/10.1130/0016-7606(1999)111<0347:VOCEAV>2.3.CO;2.
Nieva, D., Verma, M., Santoyo, E., Barragán, R.M., Portugal, E., Ortíz, J., and Quijano, L., 1987, Chemical and isotopic evidence of steam upflow and partial condensation in Los Azufres Reservoir: Proceedings of 12th Workshop on Geothermal Reservoir Engineering, Stanford University, Stanford, California, 20–22 January 1987, p. 253–259.
Ochoa-González, G.H., Carreón-Freyre, D., Cerca, M., and López-Martínez, M., 2015, Assessment of groundwater flow in volcanic faulted areas. A study case in Querétaro, Mexico: Geofísica Internacional, v. 54, p. 199–220, https://doi.org/10.1016/j.gi.2015.04.016.
O'Nions, R.K., and Oxburgh, E.R., 1988, Helium, volatile fluxes and the development of continental crust: Earth and Planetary Science Letters, v. 90, p. 331–347, https://doi.org/10.1016/0012-821X(88)90134-3.
Palacios-García, N.B., and Martini, M., 2014, From back-arc rifting to arc accretion: The Late Jurassic–Early Cretaceous evolution of the Guerrero terrane recorded by a major provenance change in sandstones from the Sierra de los Cuarzos area, central Mexico: International Geology Review, v. 56, p. 1377–1394, https://doi.org/10.1080/00206814.2014.938367.
Pérez-Campos, X., Kim, Y., Husker, A., Davis, P.M., Clayton, R.W., Iglesias, A., Pacheco, J.F., Singh, S.K., Manea, V.C., and Gurnis, M., 2008, Horizontal subduction and truncation of the Cocos Plate beneath central Mexico: Geophysical Research Letters, v. 35, L18303, https://doi.org/10.1029/2008GL035127.
Pérez-Martínez, I., Villanueva-Estrada, R.E., Cardona-Benavides, A., Rodríguez-Díaz, A.A., Rodríguez-Salazar, M.T., and Guadalupe, J., 2020, Hydrogeochemical reconnaissance of the Atotonilco el Alto–Santa Rita geothermal system in the northeastern Chapala graben in Mexico: Geothermics, v. 83, https://doi.org/10.1016/j.geothermics.2019.101733.
Pérez-Venzor, J.A., Aranda-Gómez, J.J., McDawell, F., and Solorio-Munguía, J.G., 1996, Geología del volcán Palo Huérfano, Guanajuato, México: Revista Mexicana de Ciencias Geológicas, v. 13, p. 174–183.
Pinti, D.L., Castro, M.C., Shouakar-Stash, O., Tremblay, A., Garduño, V.H., Hall, C.M., Hélie, J.F., and Ghaleb, B., 2013, Evolution of the geothermal fluids at Los Azufres, Mexico, as traced by noble gas isotopes, $\delta^{18}O$, δD, $\delta^{13}C$ and $^{87}Sr/^{86}Sr$: Journal of Volcanology and Geothermal Research, v. 249, p. 1–11, https://doi.org/10.1016/j.jvolgeores.2012.09.006.
Plank, T., Kelley, K.A., Zimmer, M.M., Hauri, E.H., and Wallace, P.J., 2013, Why do mafic arc magmas contain ~4 wt% water on average?: Earth and Planetary Science Letters, v. 364, p. 168–179, https://doi.org/10.1016/j.epsl.2012.11.044.
Ray, M.C., Hilton, D.R., Muñoz, J., Fischer, T.P., and Shaw, A.M., 2009, The effects of volatile recycling, degassing and crustal contamination on the helium and carbon geochemistry of hydrothermal fluids from the Southern Volcanic Zone of Chile: Chemical Geology, v. 266, p. 38–49, https://doi.org/10.1016/j.chemgeo.2008.12.026.
Rizzo, A.L., Barberi, F., Carapezza, M.L., Di Piazza, A., Francalanci, L., Sortino, F., and D'Alessandro, W., 2015. New mafic magma refilling a quiescent volcano: Evidence from He-Ne-Ar isotopes during the 2011–2012 unrest at Santorini, Greece: Geochemistry, Geophysics, Geosystems, v. 16, p. 798–814, https://doi.org/10.1002/2014GC005653.
Rudnick, R.L., and Gao, S., 2003, The composition of the continental crust, *in* Holland, H.D., and Turekian, K.K., eds., Treatise on Geochemistry, Vol. 3, The Crust: Oxford, UK, Elsevier-Pergamon, p. 1–64, http://doi.org/10.1016/b0-08-043751-6/03016-4.
Sano, Y., and Wakita, H., 1985, Geographical distribution of $^{3}He/^{4}He$ ratios in Japan: implications for arc tectonics and incipient magmatism: Journal of Geophysical Research: Solid Earth, v. 90, p. 8729–8741, https://doi.org/10.1029/JB090iB10p08729.
Smith, S.P., and Kennedy, B.M., 1983, The solubility of noble gases in water and in NaCl brine: Geochimica et Cosmochimica Acta, v. 47, p. 503–515, https://doi.org/10.1016/0016-7037(83)90273-9.
Straub, S.M., Gomez-Tuena, A., Stuart, F.M., Zellmer, G.F., Espinasa-Perena, R., Cai, Y., and Iizuka, Y., 2011, Formation of hybrid arc andesites beneath thick continental crust: Earth and Planetary Science Letters, v. 303, p. 337–347, https://doi.org/10.1016/j.epsl.2011.01.013.
Tardani, D., et al., 2016, Exploring the structural controls on helium, nitrogen and carbon isotope signatures in hydrothermal fluids along an intra-arc fault system: Geochimica et Cosmochimica Acta, v. 184, p. 193–211, https://doi.org/10.1016/j.gca.2016.04.031.
Tolstikhin, I.N., and Marty, B., 1998, The evolution of terrestrial volatiles: A view from helium, neon, argon and nitrogen isotope modelling: Chemical Geology, v. 147, p. 27–52, https://doi.org/10.1016/S0009-2541(97)00170-8.
Torgersen, T., 1993, Defining the role of magmatism in extensional tectonics: Helium 3 fluxes in extensional basins: Journal of Geophysical Research: Solid Earth, v. 98, p. 16,257–16,269, https://doi.org/10.1029/93JB00891.
Torgersen, T., and Jenkins, W.J., 1982, Helium isotopes in geothermal systems: Iceland, The Geysers, Raft River and Steamboat Springs: Geochimica et Cosmochimica Acta, v. 46, p. 739–748, https://doi.org/10.1016/0016-7037(82)90025-4.
Torgersen, T., Drenkard, S., Stute, M., Schlosser, P., and Shapiro, A., 1995, Mantle helium in ground waters of eastern North America: Time and space constraints on sources: Geology, v. 23, p. 675–678, https://doi.org/10.1130/0091-7613(1995)023<0675:MHIGWO>2.3.CO;2.
Urrutia-Fucugauchi, J., and Flores-Ruiz, J.H., 1996, Bouguer gravity anomalies and regional crustal structure in central Mexico: International Geology Review, v. 38, p. 176–194, https://doi.org/10.1080/00206819709465330.
Valdez-Moreno, G., Aguirre-Díaz, G.J., and López-Martínez, M., 1998, El volcán La Joya, Estados de Querétaro y Guanajuato—Un Estratovolcan miocénico del Cinturón Volcánico Mexicano: Revista Mexicana de Ciencias Geológicas, v. 15, p. 181–197.
Verma, S.P., and Carrasco-Núñez, G., 2003, Reappraisal of the geology and geochemistry of Volcán Zamorano, central Mexico: Implications for discriminating the Sierra Madre Occidental and Mexican Volcanic belt provinces: International Geology Review, v. 45, p. 724–752, https://doi.org/10.2747/0020-6814.45.8.724.
Wen, T., Pinti, D.L., Castro, M.C., López-Hernández, A., Hall, C.M., Shouakar-Stash, O., and Sandoval-Medina, F., 2018, A noble gas and $^{87}Sr/^{86}Sr$ study in fluids of the Los Azufres geothermal field, Mexico—Assessing impact of exploitation and constraining heat sources: Chemical Geology, v. 483, p. 426–441, https://doi.org/10.1016/j.chemgeo.2018.03.010.
Yardley, B.W.D., and Bodnar, R.J., 2014, Fluids in the Continental Crust: Geochemical Perspectives, v. 3, p. 1–125, https://doi.org/10.7185/geochempersp.3.1.
Zúñiga, F.R., Pacheco, J.F., Guzmán-Speziale, M., Aguirre-Díaz, G.J., Espíndola, V.H., and Nava, E., 2003, The Sanfandila earthquake sequence of 1998, Querétaro, Mexico: Activation of an undocumented fault in the northern edge of central Trans-Mexican Volcanic Belt: Tectonophysics, v. 361, p. 229–238, https://doi.org/10.1016/S0040-1951(02)00606-6.